文章编号：1001-9014(2021)03-0353-10

DOI：10. 11972/j. issn. 1001-9014. 2021. 03. 012

Sensitivity analysis of the satellite infrared hyper-spectral atmospheric sounder GIIRS on FY-4A

NONG Chuan[1,2], YIN Qiu[3*], SONG Ci[4,5], SHU Jiong[1,2]

(1. Key Laboratory of Geographic Information Science Ministry of Education, East China Normal University, Shanghai 200241, China;
2. School of Geographic Sciences, East China Normal University, Shanghai 200241, China;
3. Shanghai Meteorological Service, Shanghai 200030, China;
4. College of Science, Zhongyuan University of Technology, Zhengzhou 450007, China;
5. School of Communication and Information Engineering, Shanghai University, Shanghai 200444, China)

Abstract: Sensitivity is an important radiation performance index of remote sensor. In this paper, the sensitivity concept of infrared hyper-spectral sounding is extended from the sounder noise sensitivity to the atmospheric parameter sensitivity and the surface temperature error sensitivity for the on-orbit application of sounder. The corresponding sensitivity calculation models and their relations are introduced. These models are applied to the sensitivity evaluation of the first infrared hyper-spectral atmospheric sounder on geostationary meteorological satellite FY-4A GIIRS. With the sounder test data and the atmospheric historical statistical data, we obtained the quantitative variation characteristics of the atmospheric parameter sensitivities (atmospheric temperature, water vapor, ozone, CO_2, CH_4 and N_2O), the surface temperature error sensitivity and the sounder noise sensitivity with the channel. The physical mechanisms of these characteristics are analyzed. The results show that, as a whole, the sensitivities of atmospheric temperature, water vapor and ozone are much higher than that of the sounder noise and surface temperature error, while the sensitivities of CO_2, CH_4 and N_2O are submerged by the sounder noise sensitivity and the surface temperature error sensitivity. The study lays a foundation for the signal-to-noise ratio evaluation of infrared hyper-spectral atmospheric parameters detection, and is helpful for the optimization of infrared hyper-spectral atmospheric sounding channels.

Key words: Infrared hyper-spectral, atmospheric sounding, sounder noise sensitivity, atmospheric parameter sensitivity, surface temperature error sensitivity

FY-4A 静止气象卫星红外高光谱大气探测仪 GIIRS 探测灵敏度分析

农 川[1,2]，尹 球[3*]，宋 慈[4,5]，束 炯[1,2]

(1. 华东师范大学地理信息科学教育部重点实验室，上海 200241；
2. 华东师范大学地理科学学院，上海 200241；
3. 上海市气象局，上海 200030；
4. 中原工学院理学院，河南 郑州 450007；
5. 上海大学通信与信息工程学院，上海 200444)

摘要：灵敏度是重要的遥感器辐射性能指标。本文将红外高光谱大气探测仪仪器噪声灵敏度概念拓展，定义了面向探测仪在轨应用的大气参数灵敏度和地表温度误差灵敏度，给出了相应的计算模型和相互关系。并将之应用于第一台静止气象卫星红外高光谱大气探测仪 FY-4A GIIRS 在轨应用探测灵敏度评估。根据探测仪测试数据和大气历史统计资料，得到了大气参数(温度、水汽、臭氧、CO_2、CH_4和N_2O)、地表温度误差以及探测仪噪声灵敏度随通道的定量变化特征，分析了各变化特征的物理机制。结果表明大气温度、水汽和臭氧灵

Received date: 2020-04-14, **revised date**: 2020-07-20　　**收稿日期**：2020-04-14，**修回日期**：2020-07-20

Biography: NONG Chuan (1996-), female, Guangxi, master. Research area involves atmospheric physics and the application of meteorological satellite data. E-mail: n_chuan123@163. com.

[*] **Corresponding author**: E-mail: yinqiu@cma. gov. cn

敏度远大于探测仪噪声和地表温度误差灵敏度，而CO_2、CH_4和N_2O灵敏度被探测仪和地表温度误差灵敏度淹没。本文研究为红外高光谱大气参数探测信噪比评估奠定了基础，有助于红外高光谱大气探测通道的优选。

关 键 词：红外高光谱；大气探测；探测仪灵敏度；大气参数灵敏度；地表温度误差灵敏度

中图分类号：P4 **文献标识码**：A

Introduction

From filter to grating and interference (Optical splitting method), the number of channels for atmospheric vertical distribution detection has increased from dozens to hundreds or even thousands [1]. Since 2000, series of satellite infrared hyper-spectral atmospheric sounder (IHAS) have been developed by the United States and Europe, such as AIRS (Atmospheric Infrared Sounder) on NASA's Aqua satellite, IASI (Infrared Atmospheric Sounding Interferometer) on Metop-A/B satellite of EUMETSAT, CrIS (Cross-track Infrared Sounder) on Suomi NPP and JPSS-1 satellites [2-3]. The FY-4A meteorological satellite launched by China in 2016 is the first geostationary satellite carrying the IHAS in the world, which is the geostationary interference atmospheric vertical sounder (GIIRS)[4-6]. Later, the FY-3D, launched in 2017, also carried an IHAS named the High-spectral Infrared Atmospheric Sounder (HIRAS) [7]. With hyper-spectral resolution, good sensitivity and high-precision of spectral radiometric calibration, the IHAS has significant advantages in many applications, such as the inversion of atmospheric temperature and humidity profile, the data assimilation of numerical weather prediction, the climate change research and atmospheric trace gas detection etc.

The instrument noise sensitivity is an important performance index of remote sensor. This index is usually tested in laboratory before launched. When a satellite IHAS is putting into orbit operation, the changes of atmosphere and surface characteristics will affect its output signal.

In this paper, we extend the instrument noise sensitivity concept of the IHAS, put forward the concepts of the atmospheric parameter sensitivity and the surface temperature error sensitivity, introduce their calculation models, and apply them to evaluate the sounding sensitivity of FY-4A GIIRS. The research lays a foundation for the sounding signal-to-noise ratio (SNR) evaluation of atmospheric parameters at different spectral channels.

1 Infrared atmospheric sounding equation

When radiation transfer in the earth-atmosphere system, the atmosphere and the surface may absorb, emit and scatter radiation. The atmospheric molecular scattering and surface reflection are usually neglected for the medium and long wave infrared bands. It is assumed that radiation transfers process is not disturbed by sunlight, the atmosphere is a cloudless, plane-parallel and non-scattering medium with local thermal balance, and the surface is a black body. Taking the viewing direction to the sub-satellite point as the reference, the radiation signal received by the satellite sounder can be written as [8].

$$I_\nu = B_\nu(T_s)H_\nu(p_s) + \int_{p_s}^{0} B_\nu(T_p)\frac{dH_\nu(p)}{dp}dp \quad , \quad (1)$$

where I_ν is radiation intensity received by the sounder from the direction of the sub-satellite point. On the right-side, the first term is the contribution of the surface radiation transmitted through the atmosphere, and the second term is the contribution of the atmospheric upward radiation. ν is the wavenumber. $B_\nu(T_s)$ and $B_\nu(T_p)$ are the radiation intensities of black body with temperatures T_s and T_p respectively. T_s is the surface temperature and T_p is the atmospheric temperature at height of pressure p. $H_\nu(p_s)$ and $H_\nu(p)$ are the transmittance from the surface and from the pressure p respectively to the top of the atmosphere. p_s is the surface pressure.

According to Eq. (1), the surface temperature, the profiles of atmospheric parameters (atmospheric temperature and atmospheric absorption gases) and the wavelength determine the sounder received signal. For the convenience of sensitivity definition, we simplify Eq. (1). The details are as follows:

We use $a_j(p)(j = 1, 2, ..n)$ to represent the kinds of atmospheric absorption gases, and $a_0(p)$ for atmospheric temperature profile, Eq. (1) can be written as

$$I_\nu = F_\nu\left[T_s, \left\langle a_j(p)\right\rangle\right] \quad , \quad (2)$$

where,

$$\left\langle a_j(p)\right\rangle = \left\{a_0(p), a_1(p), \cdots a_n(p)\right\}|p = p_s \sim 0 \quad . \quad (3)$$

If $\overline{T}_s$ and $\left\langle \overline{a}_j(p)\right\rangle$ are the estimations of surface temperature and atmospheric parameter profiles, then the received signal of the sounder is estimated as $\overline{I}_\nu = F_\nu\left[\overline{T}_s, \left\langle \overline{a}_j(p)\right\rangle\right]$. Assuming that there are deviations between the actual surface temperature and atmospheric parameters and their estimations, which are δT_s and $\left\langle \delta[a_j(p)]\right\rangle$. The measurement error is ε_ν, then the deviation of the actual output signal of the sounder is as follows

$$\begin{aligned}\delta I_\nu &= I_\nu - \overline{I}_\nu + \varepsilon_\nu \\ &= F_\nu\left[T_s, \left\langle a_j(p)\right\rangle\right] - F_\nu\left[\overline{T}_s, \left\langle \overline{a}_j(p)\right\rangle\right] + \varepsilon_\nu \\ &= \left\{\frac{\partial F_\nu}{\partial T_s}\delta T_s + \sum_{j=0}^{n}\frac{\partial F_\nu}{\partial[a_j(p)]}\delta[a_j(p)]\right\} + \varepsilon_\nu\end{aligned} \quad , \quad (4)$$

where, $\frac{\partial F_\nu}{\partial T_s}\delta T_s$ and $\frac{\partial F_\nu}{\partial[a_j(p)]}\delta[a_j(p)]$ are the deviation of F_ν from $F_\nu\left[\overline{T}_s, \left\langle \overline{a}_j(p)\right\rangle\right]$ caused by δT_s and $\delta[a_j(p)]$ respectively. If the atmosphere consists of M independent layers, in which $a_j(p) = a_{ji}$ $(i = 1, 2, \cdots M)$, then

$$\frac{\partial F_\nu}{\partial [a_j(p)]}\delta[a_j(p)] = \sum_{i=1}^{M}\frac{\partial F_\nu}{\partial a_{ji}}\delta a_{ji}.$$

For an infrared hyper-spectral atmospheric sounder, if there are X detection channels in total and their central wavenumbers are ν_x ($x = 1, 2, \cdots X$), the quantities related to the wavenumber in above equations refer to the average with ν_x as the center and the spectral resolution as the bandwidth.

2 Sensitivity definitions and their calculation models

2.1 Sounder noise sensitivity

The noise sensitivity of infrared sounder is usually characterized by noise equivalent power $(NE\Delta P)_\nu$ and noise equivalent temperature difference $(NE\Delta T)_\nu$.

$(NE\Delta P)_\nu$ refers to the variation of incident infrared radiant power when the output signal change equals the root-mean-square (RMS) of sounder noise.

$$(NE\Delta P)_\nu = \Delta P\frac{\sqrt{\overline{\varepsilon_v^2}}}{\Delta V}, \quad (5)$$

where ΔP is the change of input radiant power, ΔV is its corresponding output signal change and $\sqrt{\overline{\varepsilon_v^2}}$ is the RMS of output noise.

$(NE\Delta T)_\nu$ refers to the temperature variation of black body radiation source when the output signal change equals the RMS of sounder noise.

$$(NE\Delta T)_\nu = \Delta T\frac{\sqrt{\overline{\varepsilon_v^2}}}{\Delta V}, \quad (6)$$

where ΔT is the temperature change of the black body radiation source leading to change of input radiant power ΔP.

These two indexes are calibrated with the black body whose temperature is adjustable. The results must be noted with conditions of black body temperature and wavenumber.

Supposing the $(NE\Delta P)_\nu$ and $(NE\Delta T)_\nu$ of the sounder channel with a central wavenumber ν are calibrated with a black body whose temperature is T (K), then

$$(NE\Delta T)_\nu = \frac{(NE\Delta P)_\nu}{PT(\nu,T)}, \quad (7)$$

where, $PT(\nu, T) = dB_\nu^*(T)/dT$, $B_\nu^*(T)$ is the radiation intensity at wavenumber ν emitted by a black body at temperature T (K).

If the radiant power refers to the power through unit area within unit wavenumber interval and unit solid angle range, then according to Planck's law of black body radiation, it can be proved

$$B_\nu^*(T) = \frac{C_1}{\pi}\nu^3\frac{1}{e^{C_2\nu/T}-1}, \quad (8)$$

where C_1 and C_2 are radiation constants. Therefore,

$$PT(\nu,T) = \frac{dB_\nu^*(T)}{dT} = \left[B_\nu^*(T)\right]^2\cdot\frac{\pi C_2 e^{C_2\nu/T}}{C_1\nu^2T^2}. \quad (9)$$

2.2 Atmospheric parameter sensitivity

If the estimated average state of atmospheric parameters and their RMS changes relative to the average state have been known by the statistical analysis of historical data, we can describe the atmospheric parameter sensitivity by the sensitivity of single atmospheric parameter, the comprehensive sensitivity of multiple atmospheric parameters, and the total sensitivity of atmospheric parameters.

(1) The sensitivity of single atmospheric parameter

We define the sensitivity of an atmospheric parameter as the RMS change of sounder received signal caused by the variation of this atmospheric parameter relative to its average state.

If the RMS variation of the kth atmospheric parameter $a_k(p)$ is $\sqrt{\overline{\delta[a_k(p)]^2}}$, then the sensitivity of this atmospheric parameter expressed by equivalent power is $(AE\Delta P)_{\nu k}$.

$$(AE\Delta P)_{\nu k}^2 = \overline{\left\{\begin{matrix}F_\nu\left[\overline{T}_s,\overline{a}_k(p)+\delta[a_k(p)],\left\langle\overline{a}_j(p),j\neq k\right\rangle\right]\\-F_\nu\left[\overline{T}_s,\left\langle\overline{a}_j(p)\right\rangle\right]\end{matrix}\right\}^2}$$

$$= \left\{\frac{\partial F_\nu}{\partial[a_k(p)]}\right\}^2\overline{\delta[a_k(p)]^2} \quad (k = 0,1,\cdots n), \quad (10)$$

where, $\left\{\frac{\partial F_\nu}{\partial[a_k(p)]}\right\}^2\overline{\delta[a_k(p)]^2}$ is the square deviation of F_ν from $F_\nu\left[\overline{T}_s,\left\langle\overline{a}_j(p)\right\rangle\right]$ caused by $\sqrt{\overline{\delta[a_k(p)]^2}}$, $\left\{\frac{\partial F_\nu}{\partial[a_k(p)]}\right\}^2\overline{\delta[a_k(p)]^2} = \sum_{i=1}^{M}\left(\frac{\partial F_\nu}{\partial a_{ki}}\right)^2\overline{(\delta a_{ki})^2}$.

Supposing that under the conditions of surface temperature $T_s = \overline{T}_s$ and atmospheric parameters $\left\langle a_j(p)\right\rangle = \left\langle\overline{a}_j(p)\right\rangle$, the satellite received radiation intensity is $F_\nu\left[\overline{T}_S,\left\langle\overline{a}_j(p)\right\rangle\right]$ and its corresponding equivalent black body temperature is $\overline{T}_B$, then the relations between $\overline{T}_B$ and $F_\nu\left[\overline{T}_S,\left\langle\overline{a}_j(p)\right\rangle\right]$ satisfies

$$F_\nu\left[\overline{T}_s,\left\langle\overline{a}_j(p)\right\rangle\right] = \frac{C_1}{\pi}\nu^3\frac{1}{e^{C_2\nu/\overline{T}_B}-1}. \quad (11)$$

Thus, the sensitivity of the kth atmospheric parameter represented by the equivalent temperature difference $(AE\Delta T)_{\nu k}$ is

$$(AE\Delta T)_{\nu k} = (AE\Delta P)_{\nu k}/PT(\nu,\overline{T}_B) \quad (k = 0,1,\cdots n). \quad (12)$$

In section 4, the serial number of atmospheric parameters is directly replaced by name of the atmospheric parameter. For example, atmospheric water vapor sensitivity and atmospheric temperature sensitivity characterized by equivalent temperature difference are written as $(AE\Delta T)_{\nu H_2O}$ and $(AE\Delta T)_{\nu T}$.

(2) The comprehensive sensitivity of multiple atmospheric parameters

We define the comprehensive sensitivity of multiple atmospheric parameters as the RMS change of sounder received signal caused by the variations of several atmospheric parameters.

Supposing that the combined effect of L atmospheric parameters ($l = l_1, l_2, \cdots l_L$) is considered, then the comprehensive sensitivity of these atmospheric parameters expressed by equivalent power $(AE\Delta P)_{\nu(l_1 - l_L)}$ is

$$\begin{aligned}(AE\Delta P)^2_{\nu(l_1\sim l_L)} &= \overline{\left\{\begin{array}{l}F_\nu\left[\overline{T}_s,\left\langle \overline{a}_l(p)+\delta[a_l(p)], l=l_1,l_2,\cdots l_L\right\rangle\right.\\ \qquad \left.,\left\langle \overline{a}_j(p), j\neq l_1,l_2,\cdots l_L\right\rangle\right]\\ -F_\nu\left[\overline{T}_s,\left\langle \overline{a}_j(p)\right\rangle\right]\end{array}\right\}^2} \\ &= \sum_{l=l_1}^{l_L}\left\{\frac{\partial F_\nu}{\partial[a_l(p)]}\right\}^2\overline{\delta[a_l(p)]^2} \\ &= \sum_{l=l_1}^{l_L}(AE\Delta P)^2_{\nu l}\end{aligned} \quad ,(13)$$

where, $\left\{\frac{\partial F_\nu}{\partial[a_l(p)]}\right\}^2\overline{\delta[a_l(p)]^2}$ is the square deviation of F_ν from $F_\nu\left[\overline{T}_s,\left\langle \overline{a}_j(p)\right\rangle\right]$ caused by $\sqrt{\overline{\delta[a_l(p)]^2}}$, $\left\{\frac{\partial F_\nu}{\partial[a_l(p)]}\right\}^2\overline{\delta[a_l(p)]^2} = \sum_{i=1}^{M}\left(\frac{\partial F_\nu}{\partial a_{li}}\right)^2\overline{(\delta a_{li})^2}$.

In other words, the comprehensive sensitivity of several atmospheric parameters is the root of quadratic sum of their respective sensitivities.

If there is a set of atmospheric parameters as the inversion factors and the other atmospheric parameters as the interference factors, the comprehensive sensitivity of former is called the atmospheric target sensitivity and that of the latter is called the atmospheric interference sensitivity.

(3)The total sensitivity of atmospheric parameters

The total sensitivity of atmospheric parameters refers to the comprehensive sensitivity of all atmospheric parameters. If the total sensitivity of atmospheric parameters is expressed by the equivalent power $(AE\Delta P)_{\nu all}$, then

$$\begin{aligned}(AE\Delta P)^2_{\nu all} &= \overline{\left\{\begin{array}{l}F_\nu\left[\overline{T}_s,\left\langle \overline{a}_j(p)+\delta[a_j(p)]\right\rangle\right]\\ -F_\nu\left[\overline{T}_s,\left\langle \overline{a}_j(p)\right\rangle\right]\end{array}\right\}^2} \\ &= \sum_{k=0}^{n}\left\{\frac{\partial F_\nu}{\partial[a_k(p)]}\right\}^2\overline{\delta[a_k(p)]^2} \\ &= \sum_{k=0}^{n}(AE\Delta P)^2_{\nu k}\end{aligned} \quad ,(14)$$

where, $\left\{\frac{\partial F_\nu}{\partial[a_k(p)]}\right\}^2\overline{\delta[a_k(p)]^2}$ is the square deviation of F_ν from $F_\nu\left[\overline{T}_s,\left\langle \overline{a}_j(p)\right\rangle\right]$ caused by $\sqrt{\overline{\delta[a_k(p)]^2}}$, $\left\{\frac{\partial F_\nu}{\partial[a_k(p)]}\right\}^2\overline{\delta[a_k(p)]^2} = \sum_{i=1}^{M}\left(\frac{\partial F_\nu}{\partial a_{ki}}\right)^2\overline{(\delta a_{ki})^2}$.

Obviously, the square of total sensitivity of atmospheric parameters equals the quadratic sum of the atmospheric target sensitivity and its corresponding atmospheric interference sensitivity.

$$(AE\Delta P)^2_{\nu all} = (AE\Delta P)^2_{\nu TA} + (AE\Delta P)^2_{\nu IN} \quad . \quad (15)$$

If the atmospheric parameter sensitivity is represented by the equivalent temperature difference instead of the equivalent power, Eqs. (13) ~ (15) can be rewritten as,

$$\left\{\begin{array}{l}(AE\Delta T)^2_{\nu(l_1\sim l_L)} = \sum_{l=l_1}^{l_L}(AE\Delta T)^2_{\nu l}\\ (AE\Delta T)^2_{\nu all} = \sum_{k=0}^{n}(AE\Delta T)^2_{\nu k}\\ (AE\Delta T)^2_{\nu all} = (AE\Delta T)^2_{\nu TA} + (AE\Delta T)^2_{\nu IN}\end{array}\right. . \quad (16)$$

2.3 Surface temperature error sensitivity

The surface temperature error sensitivity is defined as the RMS change of sounder received signal caused by the estimate error of surface temperature.

If the surface temperature has been determined by some methods such as infrared imager with an accuracy (RMS error) of $\sqrt{\overline{e_s^2}}$, then the surface temperature error sensitivity expressed by equivalent power $(SE\Delta P)_\nu$ is

$$\begin{aligned}(SE\Delta P)^2_\nu &= \overline{\left\{F_\nu\left[\overline{T}_s+e_s,\left\langle \overline{a}_j(p)\right\rangle\right]-F_\nu\left[\overline{T}_s,\left\langle \overline{a}_j(p)\right\rangle\right]\right\}^2} \\ &= \left\{\frac{\partial F_\nu}{\partial T_s}\right\}^2\overline{e_s^2}\end{aligned} \quad , \quad (17)$$

where, $\left\{\frac{\partial F_\nu}{\partial T_s}\right\}^2\overline{e_s^2}$ is calculated at $T_s = \overline{T}_s$, $\left\langle a_j(p)\right\rangle = \left\langle \overline{a}_j(p)\right\rangle$.

If the surface temperature error sensitivity is represented by the equivalent temperature difference $(SE\Delta T)_\nu$, then

$$(SE\Delta T)_\nu = (SE\Delta P)_\nu / PT(\nu, \overline{T_B}) \quad . \quad (18)$$

3 Data sources

3.1 FY-4A GIIRS test data

The sensitivity analysis is conducted for FY-4A GIIRS. FY-4A GIIRS is a Fourier spectrometer equipped with infrared focal plane sounder[9]. Its spectral coverage is 700~1 130 cm^{-1} (8.85~14.28 μm) for long-wave infrared band, and 1 650~2 250 cm^{-1} (4.45~6.06 μm) for medium-wave infrared band, with spectral resolution of 0.625 cm^{-1} and a total of 1 650 channels. Among them, there are 689 long-wave channels and 961 medium-wave channels [6]. Since the 2 200-2 250 cm^{-1} band is greatly affected by the solar radiation and may cause the instability of model calculation, the band ranges interested in this paper are 700~1 130 cm^{-1} and 1 650~2 200 cm^{-1} respectively with a total of 1 570 channels, including 689 long-wave channels and 881 medium-wave channels.

3.2 Other data

Atmospheric temperature profile, water vapor profile and ozone profile are obtained from the global reanalysis product ERA-Interim (http://apps.ecmwf.int/datasets/) of ECMWF (European Centre for Medium-Range Weather Forecasts). The product contains 38-year data (1979~2016) in geographical range from 20°E to 180°E and from 80°S to 80°N with 2.5°×2.5° spatial resolution. There are 10512 grid points and 37 layers in vertical direction from 1 000 hPa to 1 hPa.

We use the monthly averaged global atmosphere data to analyze the spatial and temporal changes of atmospheric temperature, water vapor and ozone. The global spatial and temporal changes of these atmospheric parameters in a month are dominated by the spatial change. Taking January 1979 and July 2016 as examples, whether the temporal variation in a month is taken into account leads to a RMS relative difference of 3.92% (Jan 1979)/1.97% (July 2016) for evaluating the standard deviation profile of atmospheric temperature from 1hPa to 1 000 hPa. As for atmospheric water vapor and atmospheric ozone, the RMS relative difference are 12.17% /10.25% and 4.90% /6.12% respectively. Taking the month to month variation in one year and the year to year variation in 38 years into account, the overall relatively errors caused by applying monthly averaged global data are under several percent.

The average profiles and the standard deviation profiles of these three atmospheric parameters are calculated. The results for atmosphere temperature have been published[10].

According to 2017 WMO (World Meteorological Organization) greenhouse gas bulletin[11], the estimated concentrations of carbon dioxide (CO_2), methane (CH_4) and nitrous oxide (N_2O) are updated to the 2016' data, and their standard deviation are based on mean annual absolute increased during last 10 years. The accuracy of estimated surface temperature is taken as 1 K.

3.3 Data application method

The sounder received radiation intensity is calculated by the Line-by-Line Radiative Transfer Model (LBLRTM), which is an accurate line-by-line integral calculation program[12-14] to calculate atmospheric molecule absorption in narrow spectral bands[15] with an accuracy of 0.5%.

For details, the reference atmosphere state and the variation distribution of atmosphere state in Eqs. (10) ~ (18) is set to be the global statistical average profiles and the global statistical standard deviation profiles for atmospheric temperature, water vapor and ozone, and is given by section 3.1 for atmospheric trace gases CO_2, CH_4 and N_2O.

All sensitivity indexes are represented by the equivalent temperature differences.

4 Results

4.1 Sounder noise sensitivity

In the laboratory test of FY-4A GIIRS noise sensitivity, the black body temperature is set to 300 K, and the optical interference signal is recorded under this radiation source condition. By means of Fourier inversion, the output spectral response to the input black body radiation is determined, from which the noise equivalent power of each channel is extracted.

The test result of $(NE\Delta P)_\nu$ and the corresponding $(NE\Delta T)_\nu$ are shown in Fig. 1. From Fig. 1:

1) There are some channels in long-wave band, their $(NE\Delta P)_\nu$ and $(NE\Delta T)_\nu$ are higher than those of surrounding channels. These higher noise channels are specifically centered on 750 cm^{-1}, 815.625 cm^{-1}, 880.625 cm^{-1}, 945.625 cm^{-1}, 1 011.25 cm^{-1} and 1 076.25 cm^{-1} plus 1~2 channels on the left and right. Their maximum $(NE\Delta P)_\nu$ and $(NE\Delta T)_\nu$ are 2 to 4 times as much as those of surrounding channels. In addition, the wavenumber intervals of peak noise channel are about 65±0.625 cm^{-1}. According to the analysis of FY-4A GIIRS development team, the abnormal $(NE\Delta P)_\nu$ or $(NE\Delta T)_\nu$ of these channels is likely to be related to the environment electrical disturbance during the sensitivity test. The disturbance does not exist when satellite is on-orbit. This problem has been solved in the FY-4B GIIRS laboratory test.

2) Excluding these channels with abnormal noises from the sounder noise sensitivity test data, the basic trend of $(NE\Delta P)_\nu$ and $(NE\Delta T)_\nu$ with the central wavenumber in the long-wave band is to decrease from 0.10 mW/(m^2·sr·cm^{-1}) and 0.12 K at 700 cm^{-1} to 0.03 mW/(m^2·sr·cm^{-1}) and 0.04 K at 900.625 cm^{-1}, then to increase to 0.17 mW/(m^2·sr·cm^{-1}) and 0.24 K at 1 129.375 cm^{-1}. As for each specific channel, the sensitivity deviates compared with basic characteristics. The standard deviations of entire long-wave band channels are 0.03 mW/(m^2·sr·cm^{-1}) and 0.04 K respectively.

3) There are no abnormal sensitivity channels in the medium-wave band.

4) In the medium-wave band, the $(NE\Delta P)_\nu$ is obviously smaller than that in the long-wave band and is basically unchanged with the increase of central wavenumber and its mean and standard deviation are 0.02 mW/(m^2·sr·cm^{-1}) and 0.01 mW/(m^2·sr·cm^{-1}), respectively.

5) The $(NE\Delta T)_\nu$ of medium-wave channels are roughly on the same level of long-wave channels. Its basic characteristic is to increase with the central wavenumber, from 0.11 K at 1 650 cm^{-1} to 0.28 K at 2 200 cm^{-1}. The standard deviation from basic change feature is 0.04 K.

4.2 Atmospheric component sensitivity

4.2.1 Atmospheric water vapor sensitivity

Atmospheric water vapor has 6.3 μm absorption band, ranging from 1 200 cm^{-1} to 2 000 cm^{-1}. Continuous absorption of water vapor exists in the atmospheric window 800-1 200 cm^{-1}. The calculated results of water vapor sensitivity for FY-4A spectral channels are shown in Fig. 2, Tables 1 and 2. Fig. 3 shows water vapor sensitivity when only water vapor is taken into account for atmosphere absorption components.

It can be seen from Figs. 2 and 3, Tables 1 and 2:

1) The variation trend of water vapor sensitivity in long-wave band:

The water vapor continuous absorption in 8~14 μm

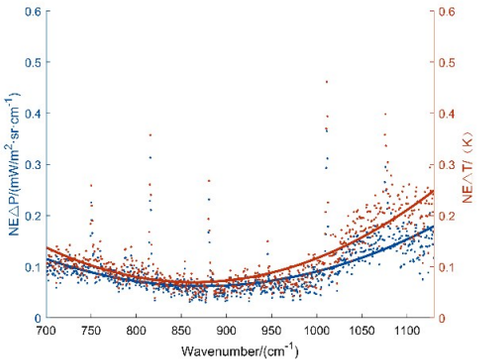

（a）

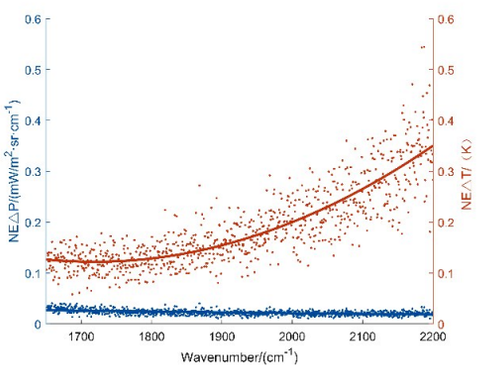

（b）

Fig. 1 The FY-4A GIIRS sounder noise sensitivity @300K for (a) long-wave band and (b) medium-wave band

图1 FY-4A GIIRS (a)长波段探测仪噪声灵敏度@300K和(b)中波段探测仪噪声灵敏度@300K

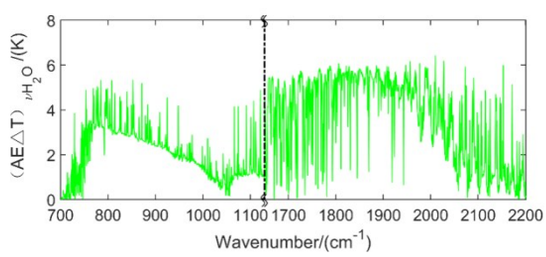

Fig. 2 The change of atmospheric water vapor sensitivity $(AE\Delta T)_{\nu H_2O}$ with the FY-4A GIIRS channels

图2 大气水汽灵敏度 $(AE\Delta T)_{\nu H_2O}$ 随FY-4A GIIRS通道的变化

band makes the water vapor sensitivity increasing from 0.94 K @ 1 130 cm^{-1} to 4.75 K @ 700 cm^{-1}. However, due to the strong absorption of CO_2 at 15 μm band, the water vapor sensitivity decreases rapidly from 4.04 K @ 800 cm^{-1} to about zero @ 700 cm^{-1}. As can be seen from Table 1, the slope is about 0.05K/cm^{-1}, and due to the ozone absorption at 9.6 μm band, a water vapor sensitivity valley is formed near 1 050 cm^{-1}, which is about 0.94 K.

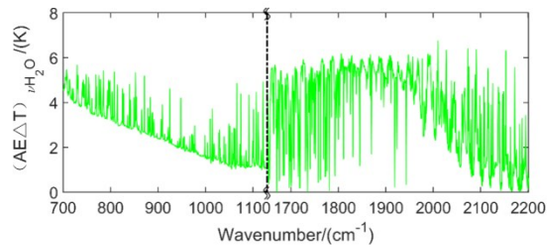

Fig. 3 Atmospheric water vapor sensitivity $(AE\Delta T)_{\nu H_2O}$ when only water vapor is taken into account for atmospheric absorption components

图3 大气吸收成分只考虑水汽时的大气水汽灵敏度 $(AE\Delta T)_{\nu H_2O}$

2) The variation trend of water vapor sensitivity in medium-wave band

The water vapor absorption at 6.3 μm band makes the water vapor sensitivity of 1 650-2 000 cm^{-1} high with an average value of 4.60 K. The water vapor sensitivity decreases rapidly from 2 000 cm^{-1} to 2 200 cm^{-1}. The strong ozone absorption at 4.75 μm band and the CO_2 absorption at 5 μm band strengthened the decreasing process.

3) Comparison of the water vapor sensitivity between long-wave band and medium-wave band

The water vapor sensitivity of long-wave channels near 800 cm^{-1} and that of medium-wave channels in 1 650-2 000 cm^{-1} is high with average values of 4 K and 4.6 K respectively. The water vapor sensitivity dispersion of medium-wave channels is greater than that of long-wave channels with standard deviations of 1.21~1.36 K for medium-wave channels and 0.44~0.80 K for long-wave channels.

In a word, the basic variation trend of atmospheric water vapor sensitivity with spectral channels is mainly determined by water vapor absorption. The absorption of other gases in their absorption bands, especially the absorption of ozone and CO_2, reduces the water vapor sensitivity.

We figure out explanations as follows:

1) An atmospheric absorbing gas affects sounder received signal by affecting the atmospheric transmittance $H_\nu(p)$, $p = p_s$~0, which is relate to the gas content and height distribution characteristics. The higher the gas concentration and the larger the gas absorption coefficient for the spectral channel concerned, the lower the atmospheric transmittance and smaller the sounder signal received. If an atmospheric component has no absorption for a spectral channel, its concentration change will not be reflected on the sounder signal of this channel. Therefore, for any absorbing gas, water vapor, ozone, CO_2, N_2O, and CH_4 etc., its sensitivity distribution with spectral channels is consistent with its absorption band. The larger the absorption coefficient is, the higher the sensitivity will be.

2) When there are various kinds of absorption components in an atmosphere layer, the radiation transmittance through this layer is a product of the transmittances

Table 1 The statistical characteristics of water vapor sensitivity $(AE\Delta T)_{\nu H_2O}$ in GIIRS long-wave band
表1 GIIRS长波段水汽灵敏度 $(AE\Delta T)_{\nu H_2O}$ 统计特征

Wavenumber range (cm^{-1})	Regression slope (K/100 cm^{-1})	Sensitivity at the low end of range (K)	Sensitivity at the high end of range (K)	Standard deviation (K)
700~800	4. 67	0. 00	4. 04	0. 80
800-1 050	-1. 08	4. 04	0. 94	0. 44
1 050-1 130	0. 84	0. 94	1. 65	0. 76

Table 2 The statistical characteristics of water vapor sensitivity $(AE\Delta T)_{\nu H_2O}$ in GIIRS medium-wave band
表2 GIIRS中波段水汽灵敏度 $(AE\Delta T)_{\nu H_2O}$ 统计变化特征

Wavenumber range (cm^{-1})	Regression slope (K/100 cm^{-1})	Sensitivity at the low end of range (K)	Sensitivity at the high end of range (K)	Mean value (K)	Standard deviation (K)
1 650~2 000	-	-	-	4. 60	1. 36
2 000-2 200	-1. 49	3. 50	0. 52	-	1. 21

of each component. Therefore, if we focus on the sensitivity of a certain absorbing gas, the presence of absorption by other gases reduces its sensitivity. The negative effect of CO_2 and ozone absorption on atmospheric water vapor sensitivity is a concrete manifestation of this mechanism.

4. 2. 2 Atmospheric ozone sensitivity

Different from the water vapor, which is mainly concentrated in the troposphere, atmospheric ozone is mainly concentrated in the stratosphere and only absorbs radiation around a few wavenumbers such as 1 041 cm^{-1} etc. The calculated results of its sensitivity for FY-4A GIIRS spectral channels are shown in Fig. 4.

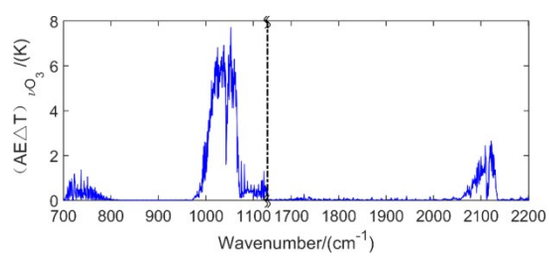

Fig. 4 The change of atmospheric ozone sensitivity $(AE\Delta T)_{\nu O_3}$ with the FY-4A GIIRS channels
图4 大气臭氧灵敏度 $(AE\Delta T)_{\nu O_3}$ 随FY-4A GIIRS通道的变化

As shown in the Fig. 4:

The ozone is most sensitive in its 9. 6 μm absorption band. For the wavenumber range of 1 000~1 068 cm^{-1}, the maximum ozone sensitivity is 7. 72 K and the average ozone sensitivity is 4. 78 K. There is an absorption band near 4. 75 μm with a sensitivity of 2. 45 K @ 2 018 cm^{-1}. In addition, there is also an absorption band near 700 cm^{-1}.

4. 2. 3 The sensitivity of atmospheric CO_2, N_2O and CH_4

Significantly different from the vertical and temporal variations of water vapor and ozone, CO_2, N_2O and CH_4 are uniformly distributed and stable in the troposphere and stratosphere.

In the FY-4A GIIRS wavenumber range, CO_2 has a strong 15 μm absorption band. There are also absorption bands of CO_2 near 10. 6 μm and 5 μm. N_2O only has a 4. 5 μm absorption band, and CH_4 has no significant absorption band, only very weak absorption around 7. 7 μm.

The sensitivity variations of these trace gases with the FY-4A GIIRS channels are shown in Figs. 5, 6 and 7.

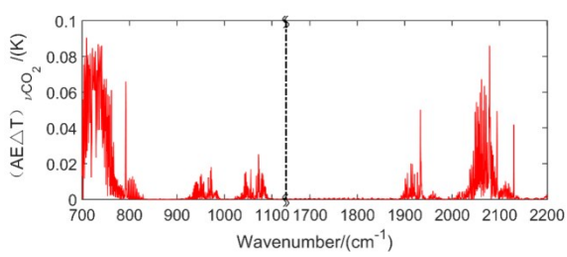

Fig. 5 The change of atmospheric CO_2 sensitivity $(AE\Delta T)_{\nu CO_2}$ with the FY-4A GIIRS channels
图5 大气CO_2灵敏度 $(AE\Delta T)_{\nu CO_2}$ 随FY-4A GIIRS通道的变化

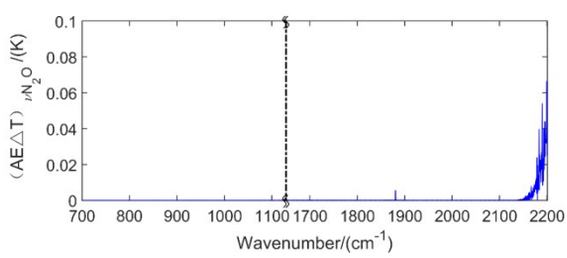

Fig. 6 The change of atmospheric N_2O sensitivity $(AE\Delta T)_{\nu N_2O}$ with the FY-4A GIIRS channel
图6 大气N_2O灵敏度 $(AE\Delta T)_{\nu N_2O}$ 随FY-4A GIIRS通道的变化

It can be seen from the figures that although CO_2 has several absorption bands such as 15 μm strong absorp-

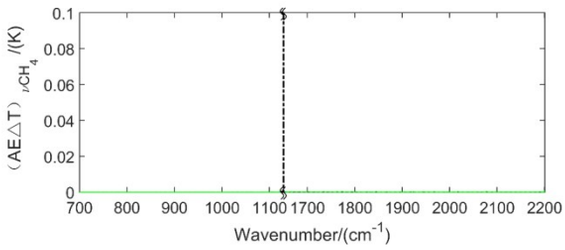

Fig. 7 The change of atmospheric CH_4 sensitivity $(AE\Delta T)_{\nu CH_4}$ with the FY-4A GIIRS channel

图7 大气CH_4灵敏度$(AE\Delta T)_{\nu CH_4}$随FY-4A GIIRS通道的变化

tion band, its sensitivity is much smaller than that of water vapor and ozone due to its stability. The maximum sensitivities of water vapor and ozone are 6.41 K and 7.72 K respectively, while the maximum sensitivity of CO_2 is only 0.09 K. Similarly, N_2O only has the maximum sensitivity at the high wavenumber end of the medium-wave band, which is only 0.04 K. As for CH_4, the sensitivity is even lower.

4.3 The atmospheric temperature sensitivity

Fig. 8 shows the change of atmospheric temperature sensitivity with FY-4A GIIRS spectral channels. Fig. 9 shows the atmospheric temperature sensitivity when only water vapor is taken into account for atmospheric absorption components.

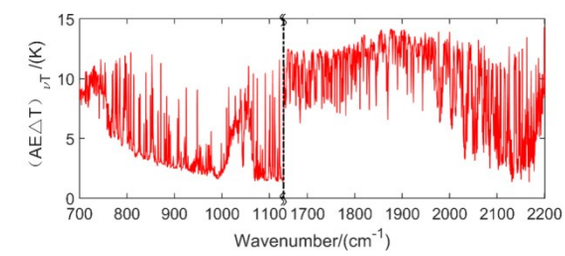

Fig. 8 The change of atmospheric temperature sensitivity $(AE\Delta T)_{\nu T}$ with the FY-4A GIIRS channels

图8 大气温度灵敏度 $(AE\Delta T)_{\nu T}$ 随FY-4A GIIRS通道的变化

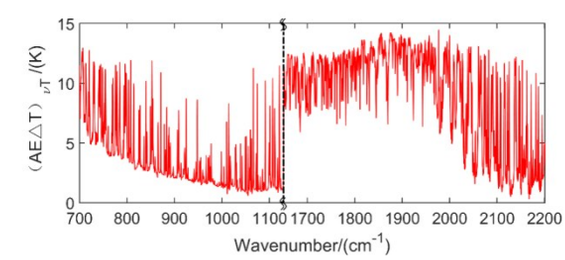

Fig. 9 Atmospheric temperature sensitivity $(AE\Delta T)_{\nu T}$ when only water vapor is taken into account for atmospheric absorption components

图9 大气吸收成份只考虑水汽时的大气温度灵敏度 $(AE\Delta T)_{\nu T}$

As can be seen from Fig. 9, when only the absorption of water vapor is taken into account, the change trend of atmospheric temperature sensitivity with spectral channels will be similar with the water vapor sensitivity. That is, as a basic situation, the higher the water vapor sensitivity, the higher the atmospheric temperature sensitivity. In the long-wave band, with the increase of wavenumber, the basic trend of atmospheric temperature sensitivity gradually decreases from an average of 10.01 K (standard deviation 1.82 K) for 700~705 cm^{-1} to an average of 1.20 K (standard deviation 0.20 K) for 1 125~1 130 cm^{-1}. In the medium-wave band, with the increase of wavenumber, the basic trend of atmospheric temperature sensitivity is stable from 1 650 cm^{-1} to 2 000 cm^{-1} with an average of 11.35 K (standard deviation 1.85 K), and gradually decreases from 2 000 cm^{-1} to 2 200 cm^{-1} with an average of 2.89 K (standard deviation 1.22 K) for 2 195 ~2 200 cm^{-1}.

However, there are other absorbing gases such as ozone, CO_2, N_2O and CH_4 in actual atmosphere. As can be seen from Fig. 8, the CO_2 15 μm absorption band and the ozone 9.6 μm absorption band increase the atmospheric temperature sensitivity in the corresponding wavenumber region of long-wave band. The CO_2 15 μm absorption band makes the atmospheric temperature sensitivity increase from an average of 7.88 K (standard deviation 2.56 K) in the case of only water vapor to an average of 9.36 K (standard deviation 0.93 K) for 700 ~ 750 cm^{-1}. The ozone 9.6 μm absorption band makes the atmospheric temperature sensitivity increased from an average of 1.96 K (standard deviation 1.68 K) in the case of only water vapor to an average of 5.46 K (standard deviation 2.07 K) for 1 000 ~ 1 068 cm^{-1}.

Similarly, for 2 000~2 200 cm^{-1} in the medium-wave band, the atmospheric temperature sensitivity also increased due to the presence of ozone, CO_2 and N_2O absorption. Atmospheric temperature sensitivity increases from an average of 5.32 K (standard deviation 3.81 K) in the case of only water vapor to 7 K (standard deviation 3.34 K).

In summary, water vapor absorption determines the basic state of atmospheric temperature sensitivity, and the presence of other absorbing gases increases the atmospheric temperature sensitivity at their absorption bands.

By comparing effects of these absorbed gases on water vapor sensitivity, their effects on atmospheric temperature sensitivity are opposite to their effects on water vapor sensitivity.

Atmospheric temperature sensitivity is positively correlated with water vapor and other gas absorption. As shown in the infrared atmospheric sounding equation Eq. (1), the atmospheric temperature profile affects sounder received signal through $B_\nu(T_p)$, $p = p_s$~0. However, it is important to note that $B_\nu(T_p)$ is always multiplied by $\frac{dH_\nu(p)}{dp}$. Which means that the atmospheric temperature playing a role affecting the sounder received signal only when there are absorbing gases. If there is no gas absorption in an atmosphere layer for a spectral channel, the atmospheric temperature change in that layer will not be reflected on the sounder received signal of this channel. The larger the concentration of a gas and the larger its ab-

sorption coefficient, the larger the response of atmospheric temperature change on the change of sounder received signal.

4.4 Surface temperature error sensitivity

The variation of surface temperature error sensitivity with FY-4A GIIRS spectral channels is shown in Fig. 10. Tables 3 and 4 respectively give the statistical mean value and standard deviation of surface temperature error sensitivity for different wavenumber ranges.

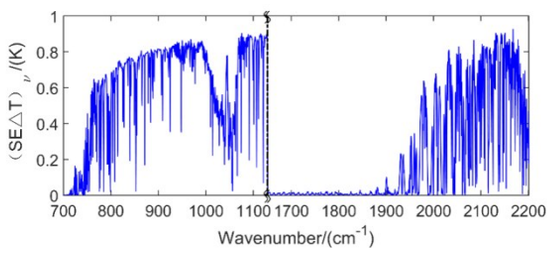

Fig. 10 The change of surface temperature error sensitivity $(SE\Delta T)_\nu$ with the FY-4A GIIRS channels
图 10 地表温度误差灵敏度 $(SE\Delta T)_\nu$ 随 FY-4A GIIRS 通道的变化

Table 3 The statistical results of the surface temperature error sensitivity $(SE\Delta T)_\nu$ for different wavenumber ranges of FY-4A GIIRS long-wave band
表 3 FY-4A GIIRS 长波段各探测通道区间地表温度误差灵敏度 $(SE\Delta T)_\nu$ 统计结果

Wavenumber range(cm^{-1})	Mean value(K)	Standard deviation (K)
700-750	0.04	0.07
750-800	0.44	0.21
800-1 000	0.74	0.13
1 000-1 068	0.50	0.17
1 068-1 130	0.80	0.16

Table 4 The statistical results of the surface temperature error sensitivity $(SE\Delta T)_\nu$ for different wavenumber ranges of FY-4A GIIRS medium-wave band
表 4 GIIRS 中波段各探测通道区间地表温度误差灵敏度 $(SE\Delta T)_\nu$ 统计结果

Wavenumber range(cm^{-1})	Mean value(K)	Standard deviation (K)
1 650-1 900	0.01	0.01
1 900-2 000	0.14	0.18
2 000-2 200	0.53	0.28

It can be seen from Fig. 10, Tables 3 and 4, the variation characteristics of surface temperature error sensitivity with spectral channels are opposite to that of atmospheric temperature sensitivity.

The reason is that, as shown by section 4.3, the stronger the atmospheric absorption is, the higher the atmospheric temperature sensitivity will be. On the contrary, according to the infrared atmospheric sounding equation Eq. (1), the change of surface temperature is reflected on the change of sounder received signal after atmospheric absorption attenuation. The atmospheric transmittance from surface to satellite sounder is determined by the contents and absorption coefficients of all kinds of absorbed gases in the whole atmosphere. The higher the gas contents and the greater the gas absorption coefficients are; the lower the surface-to-satellite atmospheric transmittance and the weaker the response of surface temperature error on sounder received signal are. If the atmosphere is completely transparent (there is no absorption at all), the change of sounder received signal will be the same as the change of surface temperature.

4.5 The comparison of different sensitivity indices

By comparing the sensitivity characteristics of atmospheric absorbing gases, atmospheric temperature and surface temperature error, we can see that:

1) The sensitivity of atmospheric water vapor and ozone are generally at levels of several degree (K), and the maximum value of the former and the latter are 6.41 K and 7.72 K respectively. The sensitive wavenumber range of ozone is limited to a narrow absorption bands such as 9.6 μm, while water vapor has a wide sensitive wavenumber coverage.

2) The sensitivity of CO_2 and N_2O are all below 0.1 K, and sensitivity of CH_4 is closer to zero. The reason is that these trace gases are very stable compared with water vapor and ozone.

3) Similar to atmospheric water vapor, atmospheric temperature has a wide sensitive wavenumber coverage, and its overall level of sensitivity is higher than that of water vapor and ozone with maximum value of 14.30 K.

4) The surface temperature error sensitivity is generally at a level of tenths degree with maximum of 0.93 K. Its variation characteristics is opposite to that of atmospheric temperature sensitivity.

5) The equivalent temperature difference of sounder noise follows the sounder itself, which varies in range of 0.04 ~ 0.54 K. As disturbing factors, contribution of the surface temperature error is generally higher than that of sounder noise, and the contributions of CO_2, N_2O and CH_4 are much less than that of surface temperature error and sounder noise.

5 Summary

In this paper, the sensitivity concept of infrared hyper-spectral atmospheric sounder is extended to atmospheric parameter sensitivity and surface temperature error sensitivity for the on-orbit application of satellite sounder. The sensitivity calculation models and their relations for different indices of atmospheric parameter sensitivity are established. The relations between equivalent power and equivalent temperature difference expressing sensitivity indices are introduced.

The sounder noise sensitivity, the sensitivity of different atmospheric parameters, and the surface temperature error sensitivity are evaluated and analyzed FY-4A GIIRS. The main conclusions are as follows:

1) The $(NE\Delta P)_\nu$ of FY-4A GIIRS in medium-wave band is obviously less than that in long-wave band, while $(NE\Delta T)_\nu$ in medium-wave band is at the same level of long-wave band whose values is under 0.55 K.

2) The sensitivities of atmospheric water vapor and that of ozone are at the same level of several degree, which is lower than that of atmospheric temperature whose maximum is about 14.3 K. The sensitive channels of atmospheric water vapor and atmospheric temperature covers wide wavenumber range, while the sensitive channels of ozone are limited to a few very narrow absorption bands.

3) The sensitivity of CO_2 and N_2O are all below 0.1 K and the sensitivity of CH_4 is close to zero, which is much lower than that of atmospheric water vapor and ozone.

4) The surface temperature error sensitivity is generally at level of a few tenths with maximum of 0.93 K. Its variation characteristic with spectral channels is opposite to that of atmospheric temperature sensitivity.

The physical mechanisms of the sensitivity evaluation results are analyzed. The main conclusions are as follows:

1) The sensitivity of an atmospheric gas is positively correlated with its own absorption strength, and negatively correlated with the absorption strengths of other atmospheric gases.

2) The sensitivity of atmospheric temperature is positively correlated with the absorption strength of every absorbing gas, while the sensitivity of surface temperature error is negatively correlated with the absorption strength of every absorbing gas.

3) The sensitivity of CO_2, N_2O and CH_4 are far lower than other atmospheric parameters, due to their contents in atmosphere are very stable.

In the follow-up works, we will analyze the signal-to-noise ratios of atmospheric temperature, water vapor and ozone by satellite infrared hyper-spectral sounding, so as to achieve the primary selection of sounding channels.

Acknowledgment

Special thanks to the FY-4A GIIRS development team of the Shanghai Institute of Technical Physics, Chinese Academy of Sciences, especially Researcher DING Lei, HUA Jian-Wen and LI Li-Bing for their support in obtaining and analyzing FY-4A GIIRS test data. This study is funded by the User Office of Meteorological Satellites of China Meteorological Administration.

References

[1] SONG Ci, YIN Qiu, XIE Ya-Nan. Development of channel selection methods for infrared atmospheric vertical sounding[J]. *Infrared*, (宋慈, 尹球, 谢亚楠. 红外大气垂直探测通道优选方法的发展. **红外**), 2019, **40**(6):18-26.

[2] QI Cheng-Li, ZHOU Fang, WU Chun-Qiang, *et al*. Spectral calibration of Fengyun-3 satellite high-spectral resolution infrared sounder [J]. *Optics and Precision Engineering*, (漆成莉, 周方, 吴春强等. 风云三号红外高光谱探测仪的光谱定标. **光学精密工程**), **27**(4), 2019.

[3] ZHOU Ai-Ming. Atmospheric Temperature and Humidity Profiles Retrieval from Hyperspectral Infrared Simulation Data Based on FY-4.(周爱明.基于风云四号高光谱红外模拟资料反演大气温湿廓线试验研究[D].南京信息工程大学),2017.

[4] Bao Y S., Wang Z J, Chen Q, *et al*. Preliminary study on atmospheric temperature profiles retrieval from GIIRS based on FT-4A satellite [J].*Aerospace Shanghai*, (鲍艳松, 汪自军, 陈强, 等. FY-4A 星 GIIRS 大气温度廓线反演模拟试验研究. **上海航天**), 2017, 34: 28-37.

[5] Dong Yao-Hai. FY-4 meteorological satellite and its application prospect[J]. *Aerospace Shanghai*(董瑶海. 风云四号气象卫星及其应用展望. **上海航天**), 2016, **33**(2): 1-8.

[6] YANG Yu-Han, YIN Qiu, SHU Jiong. Channel selection of atmosphere vertical sounder (GIIRS) onboard the FY-4A geostationary satellite[J]. *J. Infrared Millim.Waves*, (杨雨晗, 尹球, 束炯. FY-4A大气垂直探测仪(GIIRS)温度探测通道优选. **红外与毫米学报**), 2018, **37**(5):603-610.

[7] QI Cheng-Li, GU Ming-Jian, HU Xiu-Qing, *et al*. FY-3 satellite infrared high spectral sounding technique and potential application [J]. *Advanced in Meteorological Science and Technology*, (漆成莉, 顾明剑, 胡秀清,等. 风云三号卫星红外高光谱探测技术及潜在应用. **气象科技进展**), 2016, **6**(1).

[8] Liou Kuo-Nan. An Introduction to Atmospheric Radiation[M]. Beijing: China Meteorological Press. (廖国男. 大气辐射导论(第2版),北京:气象出版社),2004.

[9] GAO Cong, MAO Jian-Hua, CHEN Ren. Correction of interferogram data acquired using a focal plane FT-IR spectrometer system [J]. *Applied Optics*, 2018, **57**(10):2434-.

[10] LUO Shuang, YIN Qiu. Statistical characteristics analysis of global temperature vertical profile[J].*Journal of Tropical Meteorology*,(罗双,尹球. 全球大气温度廓线的统计特性分析[J]. **热带气象学报**),2019,**35**(4):556-566.

[11] World Meteorological Organization. WMO Greenhouse Gas Bulletin (GHG Bulletin) - No. 13: The State of Greenhouse Gases in the Atmosphere Based on Global Observations through 2016, 2078-0796 [R]. (世界气象组织 温室气体公报- 第13期:基于2016年全球观测资料的大气温室气体状况).Japan (Tokyo): WMO,2017.

[12] Clough S A, Tacono M J, Moncet J L. Line-by-line calculations of atmospheric fluxes and cooling rates: application to water vapor [J]. *J Geophys Res*, 1992, **97**(15): 761-785.

[13] Clough S A, Tacono M J. Line-by-line calculation of atmospheric fluxes and cooling rates 2. Application to carbon dioxide, ozone, methane, nitrous oxide and the halocarbons[J]. *Journal of Geophysical Research*, 1995, **100**(D8): 16519-16,535.

[14] Turner D D, Tobin D C, Clough S A, *et al*. The QME AERI LBLRTM: A closure experiment for downwelling high spectral resolution infrared radiance[J]. *Journal of the atmospheric sciences*, 2004, **61**(22).

[15] WEI He-Li, DAI Cong-Ming. Research of atmospheric transfer correction in radiance measurement: atmospheric radiative transfer model and the analysis of key atmospheric parameters[J]. *Infrared and Laser Engineering*,(魏合理,戴聪明. 辐射特性测量大气传输修正研究: 大气辐射传输模式和关键大气参数分析. **红外与激光工程**),2014,**43**(3): 885-890.